Experiment and Numerical Simulation Study on Resistance Performance of the Shallow-water Seismic Survey Vessel

Shaojuan Su[1]*,Yujie Wu [1], Yeping Xiong[2],Fangxin Guo[3],Haibo Liu[4],Qixing Cheng[3]
([1]Naval Architecture and Ocean Engineering College,Dalian Maritime University, 116026, Dalian, Liaoning, China
[2]Faculty of Engineering and Physical Sciences, University of Southampton, Boldrewood Innovation Campus, SO16 7QF Southampton, UK
[3]Dalian Hengxing Marine Engineering Design Co.,Ltd
[4]Bureau of Geophysical Prospecting(BGP),China National Petroleum Corporation(CNPC))
ssjlpz@dlmu.edu.cn

ABSTRACT: In this paper, a new type of shallow-water seismic survey vessel is proposed to solve the problem that the traditional seismic survey vessels cannot satisfy the requirements of the shallow-water marine resources exploration. To reveal the influence of shallow water effect on resistance and flow field, this research is to obtain the resistance and shallow-water characteristics of this shallow-water seismic survey vessel through ship model experiments and numerical methods. Firstly, the ship model experiment predicted the resistance at different speeds in shallow water and obtained the benchmark data to validate numerical methods. Then, the CFD methods were used to calculate the resistance of the ship in deep and shallow water. The numerical results are in good agreement with the experimental results. Finally, this paper provided details of the distribution of wave, pressure and flow fields at different water depth conditions in order to explain the causes of increased resistance in shallow water, providing a reference for the shallow-water seismic survey vessel design.
Keywords: shallow-water seismic survey vessel; ship model experiment; CFD; resistance; shallow water effect

1. Introduction

Traditional seismic survey vessels are special operation ships that are a widely used for the exploration of marine resources[1]. In recent years, with the development of global marine resource exploration, new oil and gas discoveries have been made in shallow water areas. There is an increasing demand for seismic survey vessels in the international market. However, existing seismic survey vessels are all deep-water operating vessels that cannot meet the needs of shallow-water marine resource exploration due to their heavy loads and deep drafts.

The difficulty in designing the hull form of a fat shallow draft ship lie mainly in the design of the bow and stern lines and the ability to reasonably match the parallel middle body. Due to the existence of the parallel middle body, the bow and stern lines are often too full, resulting in a strong bow bilge vortex at the steep inlet of the ship, while a large de-flow angle cause the stern streamline to separate effortlessly. A suitable bulbous bow can improve the flow field and reduce the bow bilge vortex, thus decreasing the resistance[2]. Deep-water seismic survey vessels generally use a small bulbous bow to improve the bow wave. Due to the limitations of water depth, shallow-water seismic survey vessels differ from deep-water seismic survey vessels. The small bulbous bow design of deep-water survey ships cannot be used.

When a seismic survey vessel enters the shallow water, its resistance performance and flow field characteristics are affected by the shallow water, indicating significantly different features from deep water, thus impacting resistance and safe navigation[3]. The main methods of research on the resistance of ships in shallow water are numerical simulation and ship model experiments. Lungu A et al.[4] conducted a numerical simulation of the motion of a KRISO container ship in shallow water based on the CFD method and analysed the effects of water depth on the pressure, sinkage, trim, and resistance of the ship. Aiguo et al.[5] analysed the trim and sinkage at different speeds and water depths under shallow water through numerical simulations, which improved dependable guidance for the safe operation of ships in shallow water. Saha G K et al.[6] analysed the characteristics of the resistance and viscous flow field of the KCS ship model at different water depths based on CFD. Bechthold J et al.[7] investigated the influence of different speeds on ship trim and squatting in shallow water through numerical simulation and predicted the trim and squatting of Postpanmax container ships in extremely shallow water. Pavkov M[8] studied the shallow water effect of two different trimaran models through a model experiment. Near critical speed, a large increase in resistance and sinkage was observed. Lahbib Zentari et al.[9] studied the resistance and propulsion performance of coupled pusher-barge convoys in shallow water through ship model experiment and numerical simulation, then analysed the effect of shallow water on the resistance and propulsion of the ship. The results of the ship model experiments are relatively reliable, but the experiment time and economic costs were high. In recent years, with the development of computational fluid dynamics, the use of the CFD method for shallow water performance research has become increasingly widespread. Finally, the CFD method can obtain more accurate calculation results by comparing them with experimental values.

In previous researches, the studies of ship shallow-water resistance mostly focused on numerical methods. And there are few studies using model tests and numerical methods. However, the resistance performance of shallow-water seismic survey vessels have not studied. Given the above background, this paper presents a new type of shallow-water seismic survey vessel. We propose a wide flat bulbous bow with a width that is greater than the height so that the vessel can navigate shallow water. This not only reduces the wave-making resistance of ship sailing, but also increases the proportion of the displacement volume distributed in the bow to improve the stability and seakeeping of the ship, which is conducive to resisting the heave phenomenon under the action of wind and waves[10]. The square stern, skeg, double propeller and double rudder designs are used on the stern to meet the operational requirements, solving the contradiction between the limitation of propeller diameter and propulsion power requirements in shallow water conditions. At the same time, three bow thrusters are installed in the bow to meet the needs of manoeuvrability and turning performance under shallow water. The design of skeg reduces the stern flow separation, which improves the ship's stability[11]. Ship model experiments and numerical simulation research were conducted on its resistance performance and shallow water characteristics. Analyses of the laws of ship resistance, wave-making, pressure and flow field distribution with water depth were conducted with numerical results, and the reasons for the increase of shallow water resistance are discussed, providing the basis for the prediction of shallow water resistance and the design of the shallow-water seismic survey vessel. It is significant to the study of resistance and shallow water characteristics of the shallow-water seismic survey vessel.

2. Experimental study

The research object of this paper is a new type of shallow-water seismic survey vessel. To accurately predict shallow water resistance, it is necessary to analyse shallow water working conditions through ship model resistance experiments.

2.1. A new type of shallow-water seismic survey vessel

At the beginning of the research, we designed a shallow-water seismic survey vessel based on the characteristics of a traditional seismic survey vessel and carried out CFD calculation. The initial viscous flow calculation was conducted for deep water and was a means to visualize the flow pattern along the hull and to verify whether adverse flow phenomena such as flow separation or generation of strong vortices occured.

Fig. 1. shows a large high-pressure area (red colour) at the bow, followed by low-pressure areas (blue colour) at the fore shoulder and the transition from the bow to the bottom. A low-pressure area is observed at the aft shoulder and the transition from the bottom and stern. The large difference in pressure is due to the blunt bow and full block shape of the vessel. At the blunt bow, the flow stagnates, while at the low-pressure areas the flow accelerates leading to high local frictional resistance. This phenomenon of accelerating and decelerating flow along the hull is normal for a full block ship and is not problematic so long as flow separation or flow reversal does not occur.

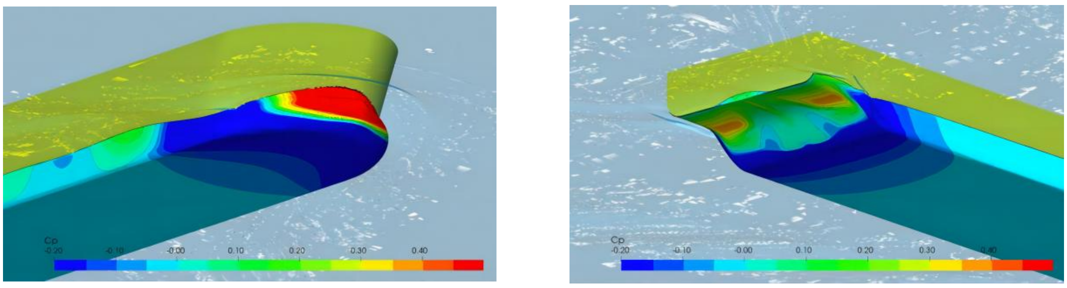

Fig. 1. Pressure distribution of original hull(10 knots, deep water)

Fig. 2. shows, however, that there are areas on the hull where flow separation occurs. At these locations, the local curvature is either too pronounced or the buttocks are too steep for the flow to follow the lines. This results in volumes of water that

stick to the hull and thus cause considerable amount of additional resistance and in case it occurs in the vicinity of the propulsors, may lead to cavitation and vibration. In the figures, the location where flow stagnation or separation occurs is shown (blue colour). The flow stagnation at the bow is caused by the blunt bow. This is no problem, because after the initial stagnation, the flow accelerates again along the hull. The curvature at the fore shoulder is, however, so pronounced that at the water line, a strong wave trough occurs and flow separation takes place again.

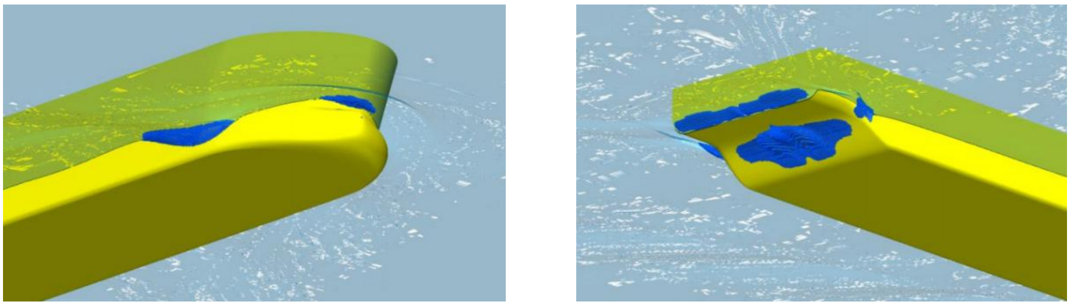

Fig. 2. Flow separation of original hull(10 knots, deep water)

The curvatures of the aft shoulder are very sudden, and flow separation occurs at the water line. In addition, the buttocks of the aft ship are too steep, and flow separation also occurs there. Besides the extra resistance, the flow separation at the aft body also negatively affects the thruster performance, as it is located in front of the two thrusters. In shallow water, the flow separation worsens. The CFD results show that the fullness of the hull is too high for a speed of 10 knots. Therefore, we decided to modify the hull to reduce the flow separation.

We propose a new type of the shallow-water seismic survey vessel. The flow separation at the fore and aft shoulder can be reduced by smoothing the curvature in those locations. The flow separation at the stern in front of the thrusters can be reduced by applying less steep buttocks and skeg. In the **Fig. 3.** the body plans of the original hull(red colour) and the modified hull(blue colour) are compared. The hull was first assessed by means of a viscous flow calculation at 10 knots in deep water to enable comparison with the results of the original hull.

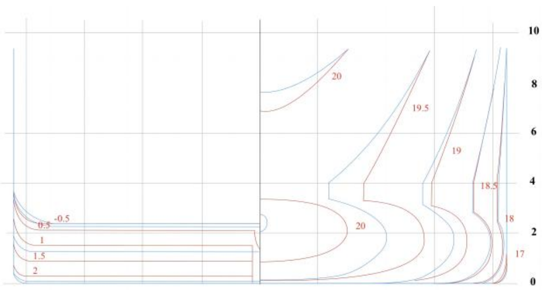

Fig. 3. lines plan of modified hull and original hull

Fig. 4. indicated a large improvement in the flow, with no flow separation at the fore shoulder and at the stern. The stagnation of flow at the bow is still present, but no change was expected at that location because the entrance angle remained the same. The vessel mostly operates in shallow-water at a speed of about 4 knots. A second viscous flow calculation was therefore conducted for the modified hull at 4 knots at a

water depth of 5m to identify the occurrence of flow separation at operational conditions. **Fig. 5.** shows that flow separation does not occur at the stern at a water depth of 5m and a speed of 4 knots.

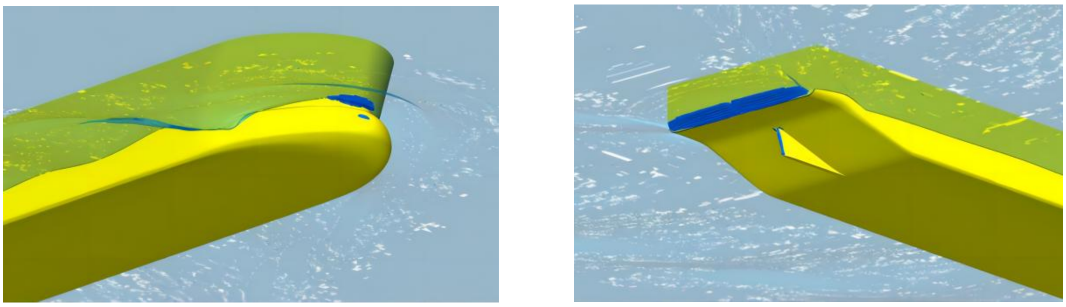

Fig. 4. Flow separation of modified hull(10 knots, deep water)

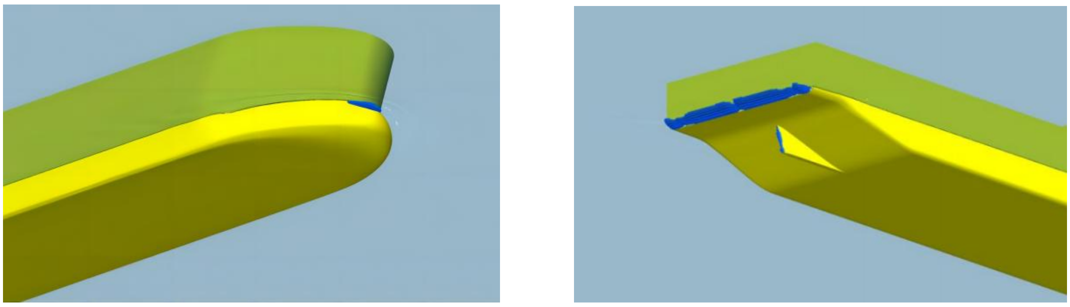

Fig. 5. Flow separation of modified hull(5 knots, 5m water depth)

Based on these results, it was decided that the ship model be based on the modified hull lines and that resistance tests be continued. **Table 1** summarizes the principal particulars of the shallow-water seismic survey vessel, and **Fig. 6.** depicts the lines plan of the ship. The shallow water resistance model experiments were performed on a scale of λ=11.641. **Fig. 7.** shows a side and bottom view of the ship's three-dimensional geometric model, and the ship model itself is shown in **Fig. 8.**

Table 1 Principal particulars of the shallow-water seismic survey vessel

Particulars	Full scale	Model
Length on waterline L_{WL} [m]	88.122	7.57
Length between perpendiculars L_{pp} [m]	84.8	7.28
Breadth B [m]	16.9	1.45
Draught T [m]	2.82	0.242
Wetted surface S [m^2]	1869	13.79
Displacement volume ∇ [m^3]	3727.8	2.363
Block coefficient C_B	0.922	0.922

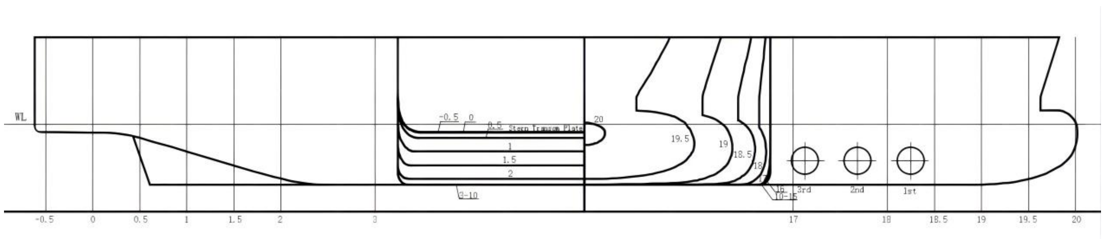

Fig. 6. Lines plan of ship

Fig. 7. Side view and bottom view of the ship's 3D model

Fig. 8. Front view and aft view of ship model

2.2. Model tests

The shallow water resistance experiments were performed in the shallow water basin at the Maritime Research Institute Netherlands (MARIN). The shallow water basin is 220 m long, 15.8 m wide, and 1.1 m deep, as shown in **Fig.9.** The shallowest working depth of the shallow-water seismic survey vessel is 5 m, the operating speed is 4-6 knots, and the free sailing speed is 10 knots. Our resistance experiments were carried out at the design draft under 5 m water conditions for seven speeds.

Fig. 9. Shallow water basin

The model was made of wood, and the surface was painted and polished. The tests were carried out under the condition of the same Froude number of the ship model and real ship. The test method for determining the resistance of ship model by changing the towing speed of the sink trailer. This test uses the photoelectric velocimeter to measure ship model speed and the pull force sensor (electric test) to measure the ship model resistance, with the towing point being placed in the floating heart. A computer data acquisition and real-time analysis system was configured on the trailer to give the test results quickly[12]. These experiment devices are shown in **Fig. 10.** During the shallow water resistance experiments, the water temperature was 17.4°C, and the water density was 998.7 kg/m3. The model was fully constrained, so that the model had no pitching and sinkage.

Fig. 10. Front view and aft view of experiment devices

2.3. experiment results

Table 2 summarises the experimental results of the tests. For each model scale speed V_m, this table lists Froude number Fr, total resistance R_{tm}, total resistance coefficient C_{tm}, friction resistance coefficient C_{fm}, and residual resistance coefficient C_{rm}. According to the Froude conversion method, the total resistance R_{tm} is divided into two parts, friction resistance R_{fm} and residual resistance R_{rm}, the residual resistance coefficients of the real ship and ship model are identical. The Froude number Fr, total resistance coefficient C_{tm}, friction resistance coefficient C_{fm} and residual resistance coefficient C_{rm} calculated by **ITTC-1957**, respectively, as follows:

$$F_r = \frac{V}{(g \cdot L_{wl})^{0.5}} \tag{1}$$

$$C_{tm} = \frac{R_{tm}}{\rho / 2 \cdot V_m^2 \cdot S} \tag{2}$$

$$C_{fm} = \frac{0.075}{(\log \mathrm{Re}_m - 2)^2} \tag{3}$$

$$C_{rs} = C_{rm} \tag{4}$$

In order to reduce the influence of tank wall and bottom on ship model test results, the results have been corrected for the tank wall effect and the scale effect[13]. A model-ship correlation allowance of C_A=0.00058 was chosen for the tests to correct the tank wall effect and the scale effect. The presented results are valid for shallow water of 5 m depth and infinite width.

Table 2 Results of resistance experiments in shallow water

V_m (m/s)	Fr	Frh	R_{tm} (N)	C_{tm}	C_{fm}	C_{rm}
0.626	0.073	0.313	19.33	0.00716	0.00331	0.00385
0.946	0.110	0.473	44.66	0.00724	0.00311	0.00413
1.110	0.129	0.555	63.20	0.00745	0.00304	0.00441
1.282	0.149	0.641	99.15	0.00876	0.00298	0.00578
1.375	0.159	0.688	130.50	0.01003	0.00295	0.00708
1.432	0.166	0.716	154.46	0.01093	0.00294	0.00799
1.474	0.171	0.737	181.74	0.01214	0.00292	0.00922

The variation of total resistance and resistance coefficient with model scale speeds are shown in **Fig.11.** and **Fig.12.** It can be seen from these graphs that with an increase in speed, the total resistance, total resistance coefficient, and residual resistance coefficient of the ship continue to increase, and the friction resistance coefficient slightly decreases. The changing trend of the residual resistance coefficient is the same as the total resistance coefficient, which is the main component affecting the change in the total resistance coefficient. This indicates that the increase in the resistance of shallow water is mainly caused by residual drag[14].

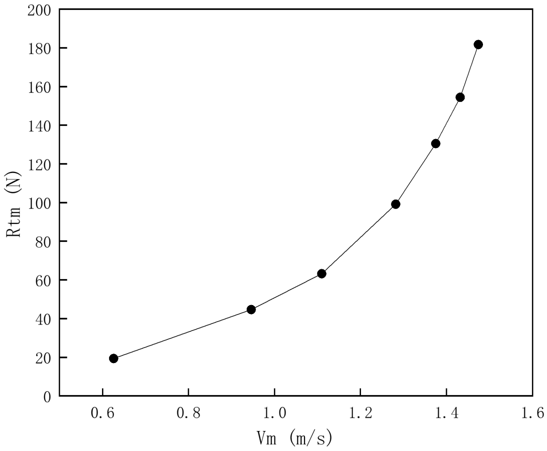

Fig. 11. Total resistance R_{tm} for different model scale speed V_m

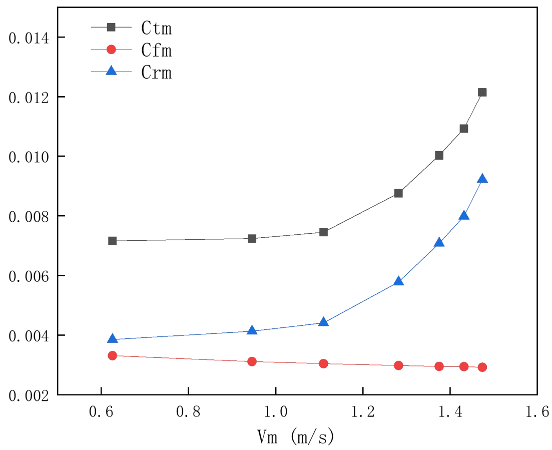

Fig. 12. Total resistance coefficient C_{tm}, friction resistance coefficient C_{fm} and residual resistance coefficient C_{rm} for different model scale speed V_m

It can be seen from formula (3) that the friction resistance coefficient decreases with the increase of the Reynolds number, while the Reynolds number increases with the increase of velocity. The coefficient of frictional resistance decreases with an increase in flow velocity, but the frictional resistance increases. According to Bernoulli's principle, when the flow velocity between the bottom of the ship and the water bottom increases, the flow velocity around the ship is more significant than that in deep water. At the same time, wave-making is more intense in shallow water, resulting in a larger wet surface area of the ship. **Fig.13.** is the free surface wave-making near the vessel at different model-scale speeds in the experiment. The graph shows that with an increase in speed, the waves around the ship gradually become more intense, and the wet surface area of the ship increases. Since the friction resistance is proportional to the wetted area of the hull, an increase in the wet surface area leads to an increase in the friction resistance.

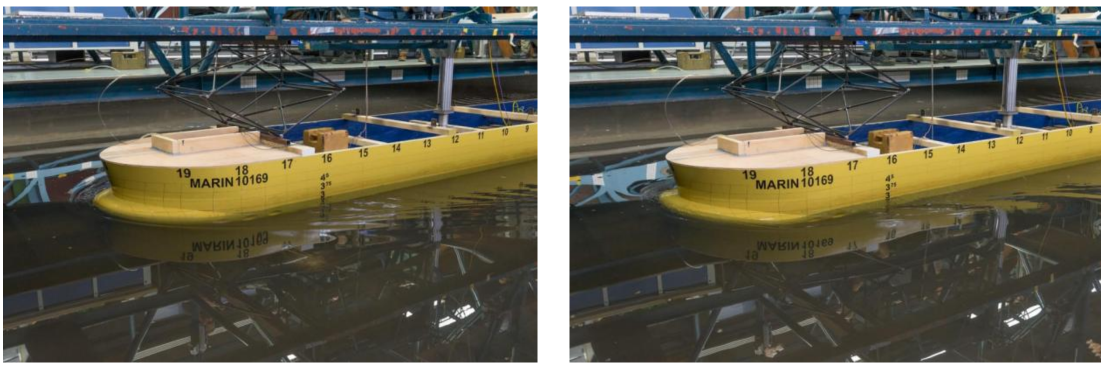

(a) Vm = 0.626m/s (b) Vm = 0.946m/s

(c) Vm = 1.110m/s

(d) Vm = 1.282m/s

(e) Vm = 1.375m/s

(f) Vm = 1.432m/s

(g) Vm = 1.474m/s

Fig. 13. Free surface at different model scale speeds

The increase in residual resistance in shallow water is mainly related to the changing of the flow field properties[15]. Due to the large block coefficient of this ship, the flow expands and accelerates in the process of moving towards the stern, increasing flow separation in shallow water. The relative velocity of the water and the ship experiences a significant increase, and the pressure drops obviously. At the same time, the gap between the stern and the water bottom becomes smaller, which makes it easy to generate vortices. This leads to an increase in viscous pressure resistance, and thus a subsequent increase in residual resistance.

3. Numerical simulation

The minimum working depth of the shallow-water seismic survey vessel is only 5 m, and the corresponding water depth to draft ratio H/T is about 1.7. It is generally believed that shallow water will influence resistance when H/T<4, and shallow water has an evident impact on resistance when H/T<2[16]. To analyse the influence of water depth on resistance and its shallow water characteristics, three water depth to draft ratios H/T were selected for numerical simulation: infinity, 3 and 1.7. The simulations are performed at model scale.

3.1 Computational domain and mesh

The method used to discretize the flow around the shallow-water seismic survey vessel was based on the numerical solution of the Reynolds-Averaged Navier-Stokes Equations (RANS) using a commercial solver STAR-CCM+. The computational domain is shown in **Fig.14.** The inlet is located $1.0L_{pp}$ in front of the ship and the outlet is placed $3.0L_{pp}$ behind the ship. The height from the free surface to the top of the domain is $1.0L_{pp}$. The side boundary is located at $2.0L_{pp}$ away from the midship plane. The bottom boundaries are located 1.7H, 3.0H, and $1.0L_{pp}$ away from the free surface, respectively.

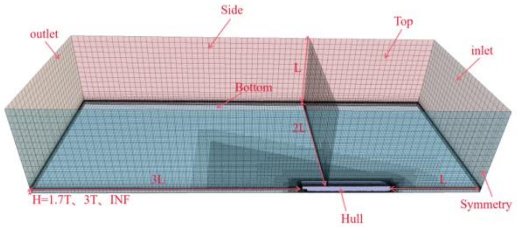

Fig. 14. Computational domain with boundaries

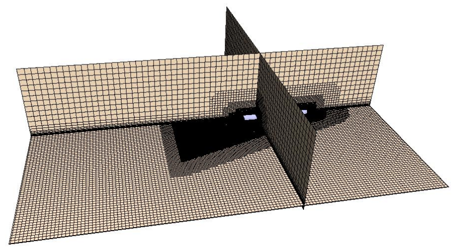

Fig. 15. Overview of the domain mesh

An internal mesh generator of STAR-CCM+ was employed. The computational domain grid is divided into a near-field zone and a far-field zone. In the near-field part, unstructured grids are used to gradually encrypt the grids near the ship (especially in the bow and stern area), free surface, and wave-making turbulence region, as shown in **Fig.15.** The structured grid was used in the far field area[17]. The six boundary layer meshes were generated with a growth rate of 1.2 near the ship in both deep and shallow water conditions. In shallow water, three boundary layer meshes are generated at the bottom boundary with a growth rate of 1.5 because of the viscosity of the water bottom. By setting the appropriate near wall thickness, the wall y + value is set between 30 and 60. In deep water, the bottom boundary is not affected by the bottom viscosity and is set to the velocity inlet.

3.2 Boundary conditions and numerical setup

Boundary conditions were applied for the simulations, as shown in **Table 3**.

Table 3 Boundary condition settings

Boundaries	Deep Water	H/T=3	H/T=1.7
Inlet	Velocity inlet	Velocity inlet	Velocity inlet
Outlet	Pressure outlet	Pressure outlet	Pressure outlet
Top	Velocity inlet	Velocity inlet	Velocity inlet
Side	Velocity inlet	Velocity inlet	Velocity inlet

Bottom	Velocity inlet	No-slip wall	No-slip wall
Hull	No-slip wall	No-slip wall	No-slip wall
Symmetry	Symmetry plane	Symmetry plane	Symmetry plane

The boundary layer formed at the bottom of the water in shallow water may affect the flow between the ship and the water bottom. Therefore, the bottom boundary is set as a no-slip wall. We used the Realizable *k-ε* model to account for turbulences. Considering the effect of the free surface, we employed the Volume of Fluid(VOF) multi-phase model to handle the free surface wave flow around the ship. The SIMPLE algorithm solver was used to solve the coupled pressure-velocity equations. The convective term is discretized in a second order up-wind scheme, while the first order scheme is used for temporal discretization. The time step satisfies the requirement that the Courant number be less than 1.

3.3 Verification and validation

The accuracy of the numerical results depends mainly on the mesh and time-step[18]. The verification and validation methods applied in this paper are based on the three-solution method proposed by Stern et al.[19] and Wilson et al.[20]. The convergence analysis was applied for the resistance in which the shallow-water seismic survey vessel met the following conditions: H/T=1.7 and V_m=1.110m/s.

The mesh convergence analysis used a refinement factor of $r = \sqrt{2}$ at the time-step t = 0.02 s. All meshes used in the study were based on a similar base size that depends on the ship length L_{pp}. The time-step convergence analysis was carried out with a refinement factor of $r = 2$ at the middle mesh S_2. According to the **ITTC** procedure[21], the difference between the calculation results of two adjacent grids can be expressed by ε, as S_i denotes the numerical calculation result and R denotes the convergence rate, which is expressed as:

$$R_i = \frac{\varepsilon_{21}}{\varepsilon_{32}} = \frac{S_2 - S_1}{S_3 - S_2} \qquad (5)$$

Where ε_{21} is the difference between the calculated results for the coarse and the medium grid. ε_{32} represents the difference between the computed results of the medium and fine meshes. Depending on the value of the convergence rate R_i, there are three possible cases of convergence: oscillatory convergence if $R_i < 0$; monotonic convergence if $0 < R_i < 1$ (MC) and divergence if $R_i > 1$.

The results of the mesh and time-step convergence analysis results are shown in **Table 4** and **Table 5**. In the tables, R_G is the mesh convergence; P_G is the accuracy order; R_T is the time-step convergence; U is uncertainty; D is the corresponding test result. Based on the results, the grid convergence rate R_G is 0.4 between 0 and 1, which is a monotonic convergence that seems acceptable. The mesh uncertainty U_G is around 1% of the test result. Compared with Grids S_1 and S_2, the error of Grid S_3 is slightly prominent, while the cells of Grid S_1 are larger. On the other hand, the time-step convergence rate R_T is less than 1, indicating that monotonic convergence is achieved for the resistance. The mesh uncertainty U_G is 0.775% of the test result, indicating a high level of numerical simulation verification. So that, the mesh and time-step uncertainty studies show that the presented numerical method has reasonably small numerical uncertainties. Considering the accuracy and efficiency, we finally chose Grid S_2 and time-step T_2 for the subsequent numerical simulation in this study. The base size is 0.146 m, the time-step is 0.02 and the number of cells in the whole calculation domain is 2.52 million.

Table 4 Mesh convergence and uncertainty analysis results

Grid	Base size (m)	Number of cells (10^6)	R_t (N)	R_G	P_G	Type	δ_G	δ_G(%D)	U_G	U_G(%D)
S_1	0.1025	6.06	67.08							
S_2	0.146	2.52	67.54	0.4	2.62	MC	0.311	0.492	0.609	0.965
S_3	0.205	1.04	68.68							

Table 5 Time-step convergence and uncertainty analysis results

	Time-step	R_t (N)	R_T	P_T	Type	δ_T	δ_T(%D)	U_T	U_T(%D)
T_1	0.01	67.01							
T_2	0.02	67.54	0.346	1.53	MC	0.281	0.445	0.489	0.775
T_3	0.04	69.07							

The numerical results were compared with experimental results to further validate the applicability of numerical simulations at different speeds[22]. **Table 6** shows a comparison of CFD results with experimental results for total resistance on shallow-water seismic survey vessel at different model scale speeds. The table shows that the total resistance values obtained from CFD agree well with the experimental data. The comparison between experimental results R_{tD} and CFD results R_{tc} at different model scale speeds shows that the maximum error E(%)[23] is less than 7%, indicating that the numerical calculation model employed in the simulation is suited for the ship resistance of shallow-water seismic survey vessels in various conditions.

Table 6 Resistance results at different model scale speeds in comparison to experimental data

V_m (m/s)	R_{tc}(N)	R_{tD}(N)	E(%)
0.626	19.33	19.64	1.6%
0.946	44.66	47.76	6.9%
1.110	63.20	67.54	6.3%
1.282	99.15	101.2	2.1%
1.375	130.50	133.68	2.4%
1.432	154.46	157.28	2.9%
1.474	181.74	187.08	1.8%

4. Numerical simulation results and analysis

The resistance and flow field of shallow-water seismic survey vessels under three different water depths are simulated in this section. Afterward, the shallow water effect and various water depths on resistance are analysed.

4.1 Comparison of resistance in deep and shallow water

Table 7 depicts the CFD computed resistance R_t, total resistance coefficient C_t, friction resistance coefficient C_f, and residual resistance coefficient C_r at different water depths and speeds. The resistance and each resistance coefficient variation with the speed and water depths are shown in **Fig. 16.** Ship resistance noticeably changes with water depth: the total resistance increases with the decrease of water depth at the same speed. With an increase in speed, the influence of water depth on resistance becomes pronounced. Under different water depths, the change in the friction resistance coefficient is not apparent, indicating that the friction resistance coefficient is not significantly affected by water depth. The residual resistance coefficient in shallow water is much larger than that in deep water, which further indicates that an increase in resistance in shallow water is directly related to enhanced residual resistance.

Table 7 Numerical results of resistance and resistance coefficient in different water depth

Water depth	V_m (m/s)	R_t (N)	C_t	C_f	C_r
H/T=INF	0.626	12.44	0.00575	0.00447	0.00128
	1.110	36.66	0.00626	0.00434	0.00192
	1.375	61.78	0.00685	0.00422	0.00262
	1.474	75.74	0.00731	0.00420	0.00311
H/T=3	0.626	17.02	0.00709	0.00453	0.00256
	1.110	50.78	0.00784	0.00447	0.00337
	1.375	84.94	0.00942	0.00437	0.00505
	1.474	103.16	0.00996	0.00435	0.00561
H/T=1.7	0.626	19.64	0.00727	0.00336	0.00391
	1.110	67.54	0.00792	0.00323	0.00469
	1.375	133.68	0.01027	0.00302	0.00725
	1.474	187.08	0.01236	0.00297	0.00939

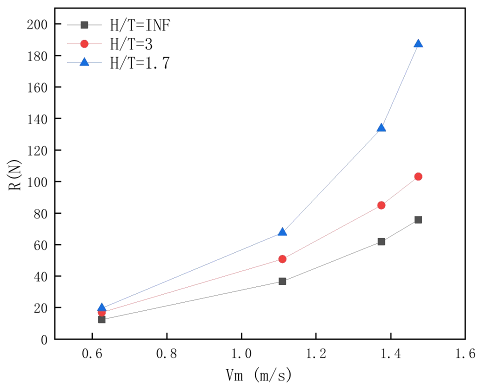

(a) Total resistance

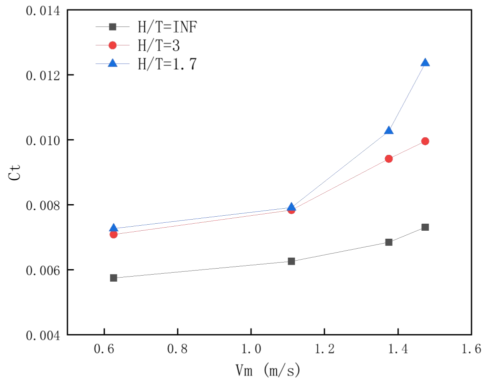

(b) Total resistance coefficient

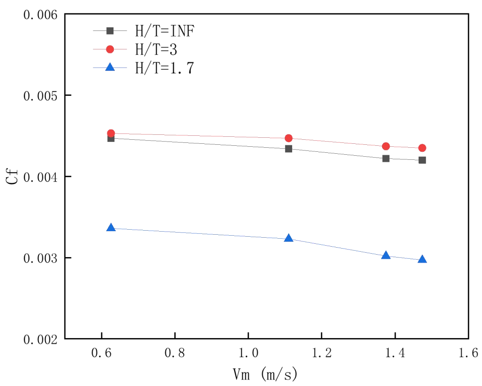

(c) Frictional resistance coefficient

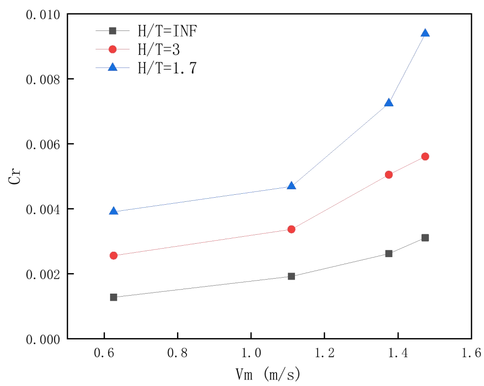

(d) Residual resistance coefficient

Fig. 16. Resistance and resistance coefficients variation with the speed and water depth

The numerical results indicate that under deep water conditions, the flow of large fat ships is easier to pass from the bottom, and the hull has a relatively small block effect on the flow. Under shallow water conditions, due to the smaller distance between the ship and the bottom of the channel, the obstruction of the flow becomes more extensive, and vortexes could possibly be created. At the same time, the ship's travelling wave becomes a shallow water wave, and wave resistance increases. Therefore, to further understand the effect of shallow water on the ship's resistance, the following paper will analyse the wave-making in shallow water.

4.2 Effect of shallow water on wave-making

The Froude depth number $Fr_h = \frac{v}{\sqrt{gh}}$, is an important parameter used to determine shallow water waves[24]. According to Fr_h, the speed can be divided into three zones: the subcritical($Fr_h < 1$), the critical($Fr_h = 1$), and the supercritical ($Fr_h >$ 1). Ships at different speeds have different wave-making properties. When a ship approaches its critical speed, the wave pattern changes intensely. The speeds we applied in this paper always corresponded to a Froude depth number of less than $Fr_h =$ 0.737. Within this range, the wave pattern in shallow water is comparable to that in deep water.

Different water depths will have a specific impact on the flow field around the hull. **Fig.17.** shows the free surface waveform of different depth waters under the operating speed. There is little difference between the wave system angle in shallow water and the Kelvin theoretical angle in deep water. In the near hull area, with the decrease in water depth, the free surface flow becomes more and more drastic, the amplitude increases, and the waveform changes are intensified, which is most apparent at the front shoulder (blue colour). In the stern wave system, the intersection line of the wave system is clear in deep water. Still, with the change in water depth, the intersection line is gradually blurred, and the attenuation of the stern shear wave in shallow water makes it impossible to distinguish the intersection line in shallow water .

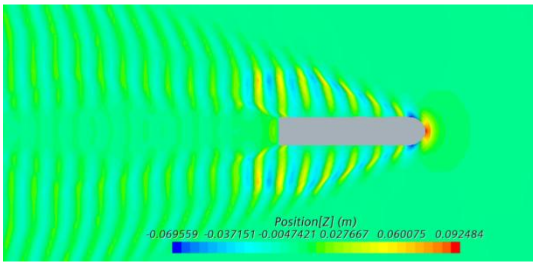

(a) H/T=INF

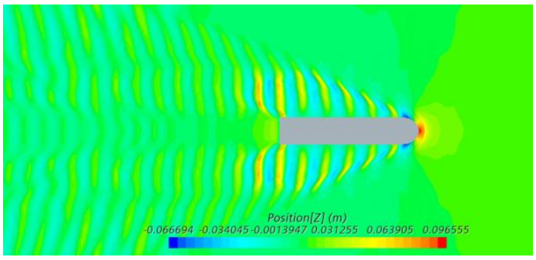

(b) H/T=3

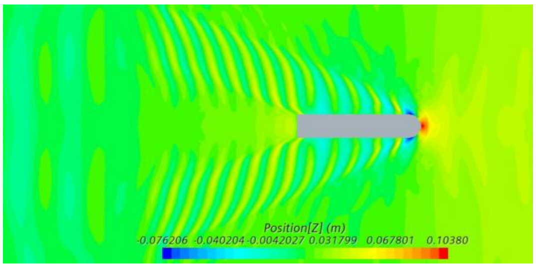

(c) H/T = 1.7

Fig. 17. Free surface wave-making at V_m=1.11m/s for different water depths

4.3 Effect of shallow water on hull pressure

The hull pressure distribution in deep water and shallow water differ. **Fig.18.** shows the pressure distribution on the hull surface at different water depths at the working speed of a shallow-water seismic survey vessel. It can be seen from the figure that the high-pressure area is formed at the bow (red colour), and a low-pressure part is formed at the fore shoulder and stern of the ship (blue colour). The pressure at the middle of the bottom is lower than that at the bow and stern. As the water depth decreases, the high-pressure area in front of the bow and the pressure difference between the bow and stern gradually increase. The two low-pressure regions in the fore shoulder and stern also gradually increase and extend to the midship, thus increasing the uneven pressure distribution of the hull.

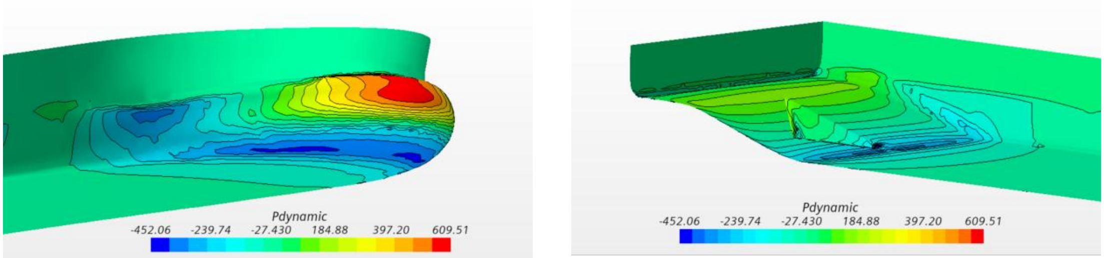

(a) H/T=INF

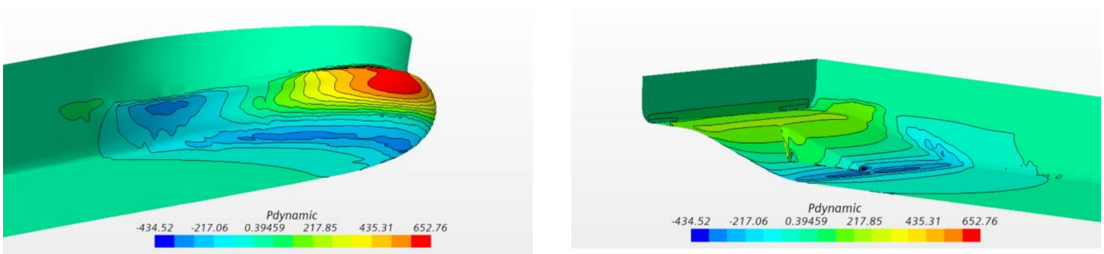

(b) H/T=3

(c) H/T = 1.7

Fig. 18. Pressure distribution on the hull at V_m= 1.11m/s for different water depths

To further understand the influence of shallow water effect on the vessels, the flow field distribution of working speed under the condition of H/T=1.7 is used as an example to analyse the causes of uneven pressure distribution on the hull. This can be seen from **Fig.19.** According to the principle of energy conservation, the flow velocity at the ship's bow is the smallest, resulting in a high-pressure area at the bow. Due to the contraction of the hull in the fore shoulder and stern, the flow velocity is accelerated, and two low-pressure areas are formed in the fore shoulder and stern. Due to the blocking effect of the hull, part of the water flows to the two sides and the direction of the ship, resulting in an increase in the flow velocity on the two sides of the ship. The flow velocity in the midship of the bottom is greater than that in the bow and stern, so the pressure in the middle of the bottom is as its lowest.

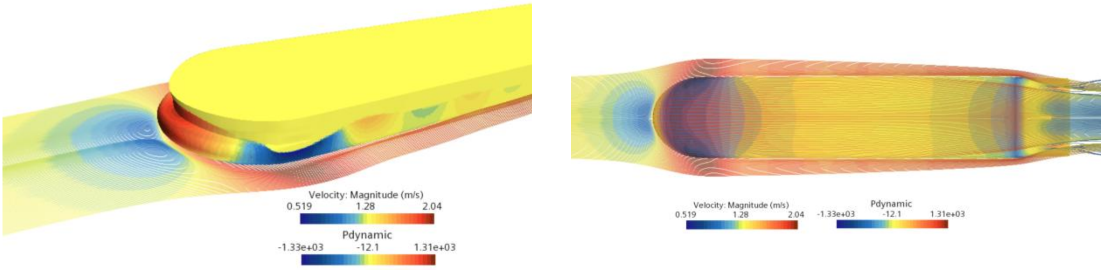

Fig. 19. Distribution of flow field and pressure with Vm=1.474m/s and H/T=1.7

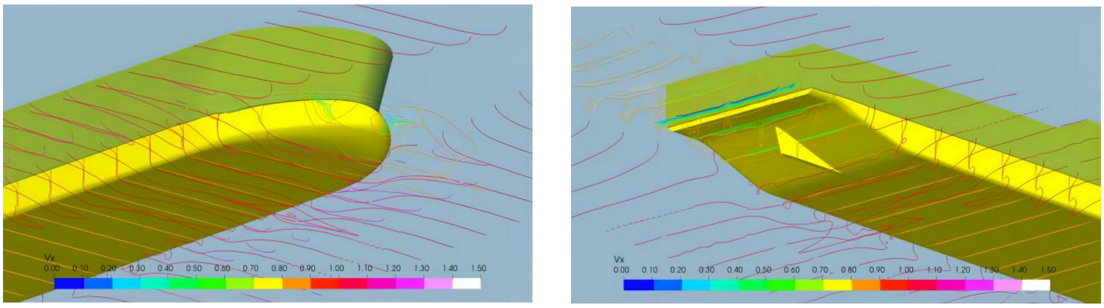

Fig. 20. Slices of axial velocity with Vm=1.110m/s and H/T=1.7

This caused high pressure at the bow and stern and low pressure in the midship. To better understand the distribution of the flow field in shallow water, **Fig.20.** shows the slices of axial velocity with *Vm*=1.110m/s and H/T=1.7. It can be seen from the figure that the water velocity is the lowest at the bow and stern. Constrained by the water depth, the water velocity between the bottom of the ship and the water increases.

5. Conclusions

To reveal the hydrodynamic characteristics of the shallow-water seismic survey vessel, this paper described a systematic experimental and numerical investigation of resistance for a shallow-water seismic survey vessel in deep and shallow waters.It provided a reference for the shallow water effect on resistance and designs of new ship types and power systems. Based on the results and analyses, the following conclusions can be drawn:

By comparing the flow separation of the original hull and modified hull, a new type of shallow-water seismic survey vessel was proposed. The modified hull performed well in shallow-water conditions, and the improvement of flow filed by the wide flat bulbous bow and skeg was verified.

Resistance experiments obtained the total resistance of the shallow-water seismic survey vessel at different speeds in shallow water. The changing level of the proportion of residual resistance corresponding to different speed conditions is considerably larger than the proportion of frictional resistance. The experiment results show that the ship was affected by the shallow water effect, which dramatically increased the residual resistance.

Numerically predicted resistances agree well with experimental results, which demonstrated the effectiveness of the numerical method used. It shows the capability of this method based on RANS to predict the resistance in deep and shallow waters for one shallow-water seismic survey. In shallow water conditions, the complexity of the flow between the hull and the bottom requires special attention regarding numerical methods.

The numerical results indicated that friction resistance is less affected by the water depth. As the water depth becomes shallower, the residual resistance increases significantly, a contrast from that in deep water. Moreover, it also provides more details about the flow fields which are definitely helpful in explaining the causes of increased resistance in shallow water.

The present study is only limited to the influence of shallow-water effect on resistance of the ship. Therefore, when the ship is working in shallow water, the phenomenon of the high pressure in the bow and stern and the low pressure in the middle of the bottom will causes the ship to sinkage and trim, which will affects the safe navigation of the ship and increase the resistance in shallow water. In the furture works, we will concentrated on the effects of sinkage and trim on resistance in different water depth conditions.

The present study is only limited to the influence of shallow-water effect on resistance of the ship. Therefore, when the ship is working in shallow water, the phenomenon of the high pressure in the bow and stern and the low pressure in the middle of the bottom will causes the ship to sinkage and trim, which will affects the safe navigation of the ship and increase the resistance in shallow water. In the furture works, we will concentrated on the effects of sinkage and trim on resistance in different water depth conditions.

References

[1] Yan, Z., Mao, Y.S., Liu, C.G., 2015. Dynamic Simulation of 12 Streamers Changeable Towed System of Seismic Survey Vessel, 3RD INTERNATIONAL CONFERENCE ON TRANSPORTATION INFORMATION AND SAFETY (ICTIS 2015), pp. 792-796.

[2] Lu, Y., Gu, Z.H., Liu, S.W., Chuang, Z.J., Li, Z.Y., Li, C.Z., 2022. Scenario-based optimization design of icebreaking bow for polar navigation. Ocean Engineering 244.

[3] Debaillon, P., 2010. Numerical Investigation to Predict Ship Squat. JOURNAL OF SHIP RESEARCH 54 (2), 133-140.

[4] Lungu, A., 2020. Numerical Simulation of the Squatting of Floating Bodies Moving in Shallow Water, 13TH INTERNATIONAL CONFERENCE INTERDISCIPLINARITY IN ENGINEERING (INTER-ENG 2019), pp. 432-439.

[5] Shi, A.G., Wu, M., Yang, B., Wang, X., Wang, Z.C., 2012. Resistance Calculation and Motions Simulation for Free Surface Ship Based on CFD, INTERNATIONAL CONFERENCE ON ADVANCES IN COMPUTATIONAL MODELING AND SIMULATION, pp. 68-74.

[6] Saha, G.K., Miazee, M.A., 2017. Numerical and Experimental Study of Resistance, Sinkage and Trim of a Container Ship, 10TH INTERNATIONAL CONFERENCE ON MARINE TECHNOLOGY (MARTEC 2016), pp. 67-73.

[7] Bechthold J, Kastens M . Robustness and quality of squat predictions in extreme shallow water conditions based on RANS-calculations[J]. Ocean Engineering, 2020, 197:106780-.

[8] Pavkov, M., Morabito, M., 2014. Experimental Investigation of Trimaran Models in Shallow Water. JOURNAL OF SHIP PRODUCTION AND DESIGN 30 (2), 66-78.
[9] Zentari, L., el Mocta, O., Lassen, J., Hallmann, R., Schellin, T.E., 2022. Experimental and numerical investigation of shallow water effects on resistance and propulsion of coupled pusher-barge convoys. Applied Ocean Research 121.
[10] Sang L , Lee S M . Experimental Study on the Towing Stability of Barges Based on Bow Shape[J]. Journal of the Korean Society of Marine Environment and Safety, 2016, 22(7):800-806.
[11] Im, N.K., Lee, S.M., Lee, C.K., 2015. The influence of skegs on course stability of a barge with a different configuration. Ocean Engineering 97, 165-174.
[12] Cuong, D., Tuan, T., 2022. Wave Hydrodynamics across Steep Platform Reefs: A Laboratory Study. Civil Engineering Journal 8, 1739-1751.
[13] Hosoda, R., 1978. Effect of Side-wall Interference of Towing Tank on the Results of Experiments in Waves (2). Journal of the Society of Naval Architects of Japan 1978 (143), 52-60.
[14] Zeng Q , Hekkenberg R , Thill C . On the viscous resistance of ships sailing in shallow water[J]. Ocean Engineering, 2019, 190:106434.
[15] Le, T.H., Vu, M.T., Bich, V.N., Phuong, N.K., Ha, N.T.H., Chuan, T.Q., Tu, T.N., 2021. Numerical investigation on the effect of trim on ship resistance by RANSE method. Applied Ocean Research 111.
[16] Mucha, P., el Moctar, O., Dettmann, T., Tenzer, M., 2018. An experimental study on the effect of confined water on resistance and propulsion of an inland waterway ship. Ocean Engineering 167, 11-22.
[17] Yamini, O.A., Movahedi, A., Mousavi, S.H., Kavianpour, M.R., Kyriakopoulos, G.L., 2022. Hydraulic Performance of Seawater Intake System Using CFD Modeling. JOURNAL OF MARINE SCIENCE AND ENGINEERING 10 (7).
[18] Zhou, L.L., Abdelwahab, H.S., Soares, C.G., 2021. Experimental and CFD investigation of the effects of a high-speed passing ship on a moored container ship. Ocean Engineering 228.
[19] Stern, F., Wilson, R.V., Coleman, H.W., Paterson, E.G., 2001. Comprehensive approach to verification and validation of CFD simulations - Part 1: Methodology and procedures. JOURNAL OF FLUIDS ENGINEERING-TRANSACTIONS OF THE ASME 123 (4), 793-802.
[20] Wilson, R., Shao, J., Stern, F., 2004. Discussion: Criticisms of the "correction factor" verification method [1]. Ibid. 126, 704-706.
[21] ITTC Procedures and Guidelines, 2008. Uncertainty Analysis in CFD Verification and Validation, 7.5-03-01-01.
[22] Kok, Z., Jin, Y.T., Chai, S.H., Denehy, S., Duffy, J., 2018. URANS prediction of berthed ship-passing ship interactions. SHIPS AND OFFSHORE STRUCTURES 13 (6), 561-574.
[23] Ghaleh, R.S., Yamini, O.A., Mousavi, S.H., Kavianpour, M.R., 2021. Numerical Modeling of Failure Mechanisms in Articulated Concrete Block Mattress as a Sustainable Coastal Protection Structure. SUSTAINABILITY 13 (22).
[24] Terziev, M., Tezdogan, T., Oguz, E., Gourlay, T., Demirel, Y.K., Incecik, A., 2018. Numerical investigation of the behaviour and performance of ships advancing through restricted shallow waters. JOURNAL OF FLUIDS AND STRUCTURES 76, 185-215.